Long-living Earthquake Swarm and Intermittent Seismicity in the Northeastern Tip of the Noto Peninsula, Japan

Y. Amezawa[1], Y. Hiramatsu[2], A. Miyakawa[1], K. Imanishi[1], and M. Otsubo[1]

[1]Geological Survey of Japan, National Institute of Advanced Industrial Science and Technology.

[2]School of Geosciences and Civil Engineering, College of Science and Technology, Kanazawa University.

Corresponding author: Yuta Amezawa (amezawa.y@aist.go.jp)

Key Points:

- An energic and long-living earthquake swarm has been observed in the northeastern tip of the Noto peninsula, Japan.
- Observed diffusive hypocenter migrations imply that pore fluid pressure migration is a driving factor of the swarm.
- Intermittent seismicity at the bottom of the initial cluster suggests that a geyser-like fluid supply is a key factor in swarm longevity.

Keywords:
earthquake swarm, hypocenter migration, fluid, diffusivity, permeability, Noto peninsula

Abstract

The factors controlling earthquake swarm duration are remain unclear, especially in the long-living ones. A severe earthquake swarm struck the tip of the Noto peninsula, Japan. Ten $M > 4.0$ earthquakes occurred, and the sequence has continued more than four years. We investigated the spatiotemporal characteristics of the swarm using relocated hypocenters to elucidate the factors causing this long duration. The swarm consists of four seismic clusters—northern, northeastern, western, and southern—the latter of which began first. Diffusive hypocenter migrations were observed in the western, northern, and northeastern clusters with moderate to low diffusivities, implying a low-permeability environment. Rapid diffusive migration associated with intermittent seismicity deep within the southern cluster suggests the presence of a highly pressurized fluid supply. We conclude that the nature of this fluid supply combined with intermittent seismicity from the southern cluster and a low-permeability environment are the key causes of this long-living swarm.

Plain Language Summary

Earthquake swarms are sequences of several earthquakes occurring in a concentrated area over a given period. Unlike other major earthquakes, which have one main shock and several subsequent aftershocks, swarms lack a clear mainshock event. The causes of long-lasting earthquake swarms are not sufficiently understood. In the northeastern tip of the Noto Peninsula in Japan, more than 20,000 earthquakes occurred between May 2018 and June 2022, including ten events over magnitude 4.0. To understand the controlling factors of this long-living earthquake swarm, we investigated the spatiotemporal characteristics of the swarm using high-resolution relocated hypocenter locations. The hypocenters of the swarm are spatially separated in four clusters and initiated from the southern cluster. We also observed a diffusive pattern in hypocenter distribution, which is typical of earthquake swarms surrounding volcanoes or fluid injection wells, implying the existence of fluid as a driving factor of the swarm. In the southern cluster specifically, we found many intermittent seismic activities with rapid diffusive changes in hypocenter distribution, suggesting the presence of a highly pressurized, deep-source fluid supply. The intermittent fluid supply from the southern cluster toward the others and the relatively low-permeability environment are key factors in the longevity of this earthquake swarm.

1 Introduction

Earthquake swarms are patterns of seismic activity that have no clear mainshock and continue for a specific period (e.g., Mogi, 1963). Swarms are often observed around volcanoes, geothermal sites, and anthropogenic fluid injection wells (e.g., Chen & Shearer, 2011; Yukutake et al., 2011, Horton 2012). Previous studies have revealed the driving factors of swarms, such as the shear strength of faults or changes in the stress state around the swarm area by highly pressurized fluid intrusion (e.g., Shelly et al., 2016; Yoshida et al., 2017), aseismic slip (e.g., Lohman & MacGuire, 2007; Dublanchet & De Barros, 2021), and magmatic dyke intrusion (e.g., Toda et al., 2002).

An important concern regarding earthquake swarms is the duration of swarm activity. Previous studies have reported plausible factors that control swarm duration, such as the distance from a volcano (Vidale et al., 2006), heterogeneity of crustal permeability (Ross et al., 2020), and diffusivity of hypocenter migration as a function of crustal permeability (Amezawa et al., 2021). The duration of an earthquake swarm can range from a few days to several years. Swarms spanning several years have been reported, such as the Matsushiro, Japan swarm (e.g., Hagiwara & Iwata, 1968; Cappa et al., 2009), the Ubaye Valley, French Alps swarm (Jenatton et al., 2007; Thouvenot et al., 2016), the Cahuilla Valley, USA swarm (Hauksson et al., 2019; Ross et al., 2020), the Tohoku, Japan swarms (Amezawa et al., 2021), and swarms in Southern California (Ross & Cochran, 2021). Understanding the causes of earthquake swarm longevity is an important step in elucidating the overall nature of earthquake swarms and assessing the risk to human life when a swarm area is close to anthropogenic activity.

In this study, we examined the driving mechanisms of a long-living earthquake swarm in the northeastern tip of the Noto Peninsula in central Japan (Figure 1). The swarm activity began in June 2018 and has continued for over four years. More than 20,000 earthquakes, including three $M \geq 5.0$ events, were detected within a 15 km^2 area at the tip of the peninsula. The activity drastically increased in December 2020, and three novel seismic clusters formed in the western, northern, and northeastern areas adjacent to the initial cluster (hereafter referred to as the W, N, NE, and S clusters, respectively) (Figure 1). The largest earthquake recorded during this timeframe (*M*5.4) occurred on 19 June 2022 at the west rim of the NE cluster. The focal mechanisms provided by the F-net moment tensor catalog (National Research Institute for Earth Science and Disaster Resilience, 2019a) indicate mostly reverse faults with northwest-southeast compression. These focal mechanisms are comparable to the regional reverse fault-dominated stress field (Terakawa & Matsu'ura, 2010). To reveal the mechanisms perpetuating this long-living swarm, we performed a detailed analysis of the spatiotemporal change in hypocenter distribution using a high-resolution relocated hypocenter catalog.

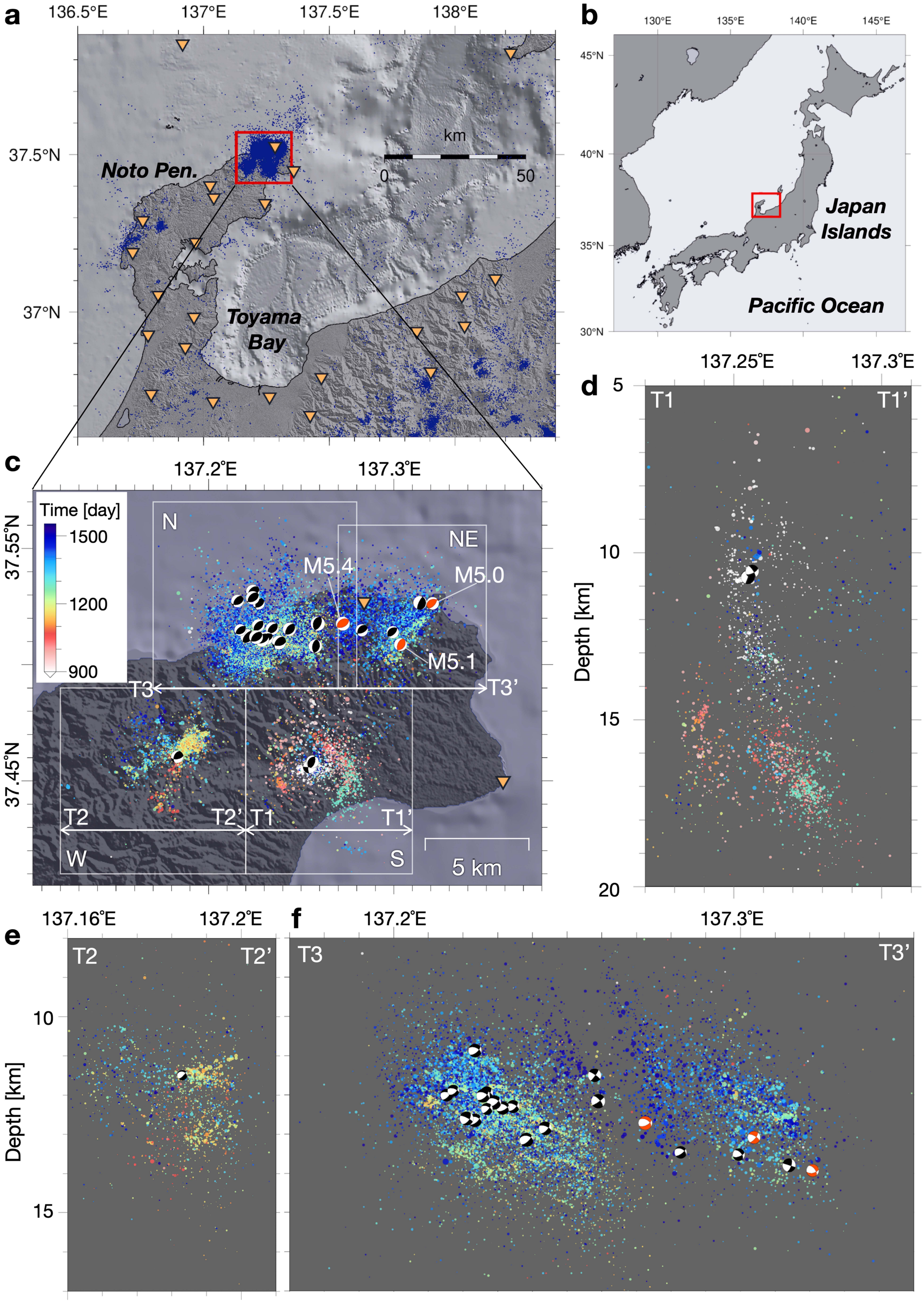

93

94 **Figure 1.** Hypocenter distribution of the earthquake swarm in the northeastern of the Noto

95 peninsula earthquake swarm. **a** Regional map of the study area. Red rectangle indicates the

swarm area. Blue dots show the seismicity between May 2018 and June 2022 from the unified catalog of the Japan Meteorological Agency. Orange inverse triangles represent seismic stations used in this study. **b** Index map. **c** Areal map of the study area. Colored dots show the relocated epicenter distribution of the swarm, displayed in order of the elapsed days from 13 May 2018. White rectangles delineate cluster borders (S, W, N, and NE clusters). Bidirectional arrows indicate the cross-section lines (T1–T1′, T2–T2′, T3–T3′) corresponding to **d**, **e**, and **f**, respectively. Black and red beach balls represent the F-net focal mechanism solutions for $4.0 \leq M < 5.0$ and $M \geq 5.0$, respectively. **d–f** Cross-sectional views for the S, W, and N-NE clusters respectively.

2 Data and Methods

2.1 Hypocenter Relocation

We used the double-difference algorithm (Waldhauser & Ellsworth, 2000) to relocate the hypocenters of 20,542 events detected in the swarm area by the Japan Meteorological Agency (JMA) between January 2018 and June 2022. The magnitudes of the relocated events were greater than or equal to 0.0. We prepared differential-time data using both the travel-time data taken from the unified catalog of JMA and cross-correlation delay times. Calculations using the JMA catalog yielded 497,446 and 490,057 differential-time data for *P* and *S* wave, respectively. The number of differential-time data calculated using the *P* and *S* waveform cross-correlation delay times was 373,090 and 481,843, respectively. To calculate the cross-correlation, we gathered data on the vertical component waveforms from at least six stations around the swarm area and applied a bandpass filter between 5 and 10 Hz. The time window for *P* and *S* waves was before and after 1.0 s of the theoretical travel time. We calculated the cross-correlation function for all event pairs and adopted delay times with the maximum correlation as differential-times. The lower limit of the cross-correlation coefficient was 0.8. We used the JMA2001 1-D velocity model (Ueno, 2002), which is routinely used at the JMA for hypocenter determination in Japan. We performed 30 iterations of hypocenter relocation. In the first half of the iterations, the catalog data were weighted 100 times higher than the cross-correlation data to constrain the relative locations of the hypocenters. In the second half of the iterations, we weighted the cross-correlation data 100 times higher than the catalog data to constrain fine-scale structures.

2.2 Evaluation of Hypocenter Migration

To determine the hypocenter migration features for comparison with earthquake swarms in other regions, we estimated the diffusivity of hypocenter migration by fitting an isotropic pore-fluid pressure diffusion model proposed by Shapiro et al. (1997). According to this model, the front line of hypocenter migration can be represented as follows:

$$r = \sqrt{4\pi D t} \quad (1)$$

where *r* [m] is the distance from the diffusion origin, *t* [s] is the elapsed time from the beginning of diffusion, and *D* [m^2/s] is the hydraulic diffusivity. For model fitting, we followed the procedure of Amezawa et al. (2021), which stably estimated the diffusivity of multiple swarms in northeastern Japan using unified criteria. Using equation (1), the diffusivity *D* was estimated by linear regression. The data in the 95th percentile for distance were calculated for events that occurred in a 30-day moving time bin that overlapped by a day. During curve-fitting, we found that some hypocenter migrations ceased in the middle of the sequence (Figure 2(a), 2(c)). To address this, we considered their end-time to be the date when the cumulative number of events in each cluster reached 30% of the total.

For theoretical curve fitting, we needed to determine the spatial and temporal origins of hypocenter migration. Because the true diffusion origin was unknown, we employed a grid search algorithm to identify it. We separated the swarm area (Figure 2) into 0.01° × 0.01° × 1.0 km spatial grid points, and prepared temporal origin candidates as the time before the origin time of the first event in each cluster. The temporal origin was searched in five-day increments within the range of 0 to 15 days before the first event in each cluster. We then performed theoretical curve fitting on all diffusion origin candidates to identify the best-fitting result.

3 Results

We successfully relocated 99% of the initial hypocenters (20,399 events). The differential time residuals for the catalog data and cross-correlation data decreased from 134 to 53 ms and from 251 to 4 ms, respectively. The relocated hypocenter locations revealed the spatiotemporal development of the swarm in detail (Figure 1, Movie S1 in Supporting Information). Seismic activity initiated deep within (10–15 km) the S cluster and continued for approximately two years in almost the same area. On 27–28 December 2020, numerous small earthquakes suddenly occurred deeper (15–20 km) within the S cluster, followed by three novel, swarm-like sequences in areas 5 km west, north, and northeast of the S cluster (W, N, and NE cluster, respectively).

The seismicity characteristics between each cluster are quite different. In the S cluster, small earthquakes ($M \leq 2.0$) were predominant, and seismic activity was intermittent. The notable features of the hypocenter distribution in this cluster were deep activity (10–20 km) and a corn-like shape (Figure 1(c), 1(d), and Movie S2 Supporting Information). The W cluster was also composed of earthquakes of $M \leq 2.0$ (Figure 1(c), 1(e)), but showed continuous seismic activity. The seismicity in the N cluster was consistently energetic, involving more than 10 earthquakes of $M \geq 4.0$. The hypocenter distribution showed many parallel planes approximately 1 km in length striking northeast-southwest and dipping approximately 45° to the east side (Figure 1(c), 1(f), and Movie S3 in Supporting Information). Seismicity in the NE cluster was relatively quiet from January to July 2021 (predominantly $M \leq 2.0$ earthquakes), but not long after, six $M \geq 4.0$ occurred, including an *M*5.1 earthquake on 16 September 2021, an *M*5.4 on 19 July 2022, and an *M*5.0 on 20 June 2022 (Figure 1(c), 1(f)).

Diffusive hypocenter migrations were observed over the entire period in the W, N, and NE clusters (Figure 2). The hypocenter migration diffusivities in the W, N, and NE clusters were estimated to be ($9.8 \times 10^{-2} \pm 5.3 \times 10^{-3}$ m^2/s), ($9.4 \times 10^{-2} \pm 4.7 \times 10^{-3}$ m^2/s), and ($1.2 \times 10^{-1} \pm 3.2 \times 10^{-3}$ m^2/s), respectively. The locations of the diffusion origins are shown in Figure 2(d–f). The time origins were estimated to be 15 days before the first event in any cluster. Although we could not observe clear diffusive migration throughout the entire period of the S cluster, many intermittent activities with diffusive migration were observed (Figure 3). We roughly estimated the diffusivities of these migrations from each first event using the diffusion model (Equation

(1)). Figure 3(b–i) shows examples of intermittent seismic activities, and we found rapid diffusive migrations with very high diffusivity (e.g., $D = 2.0 \times 10^2$ m^2/s) (Figure 3(e)).

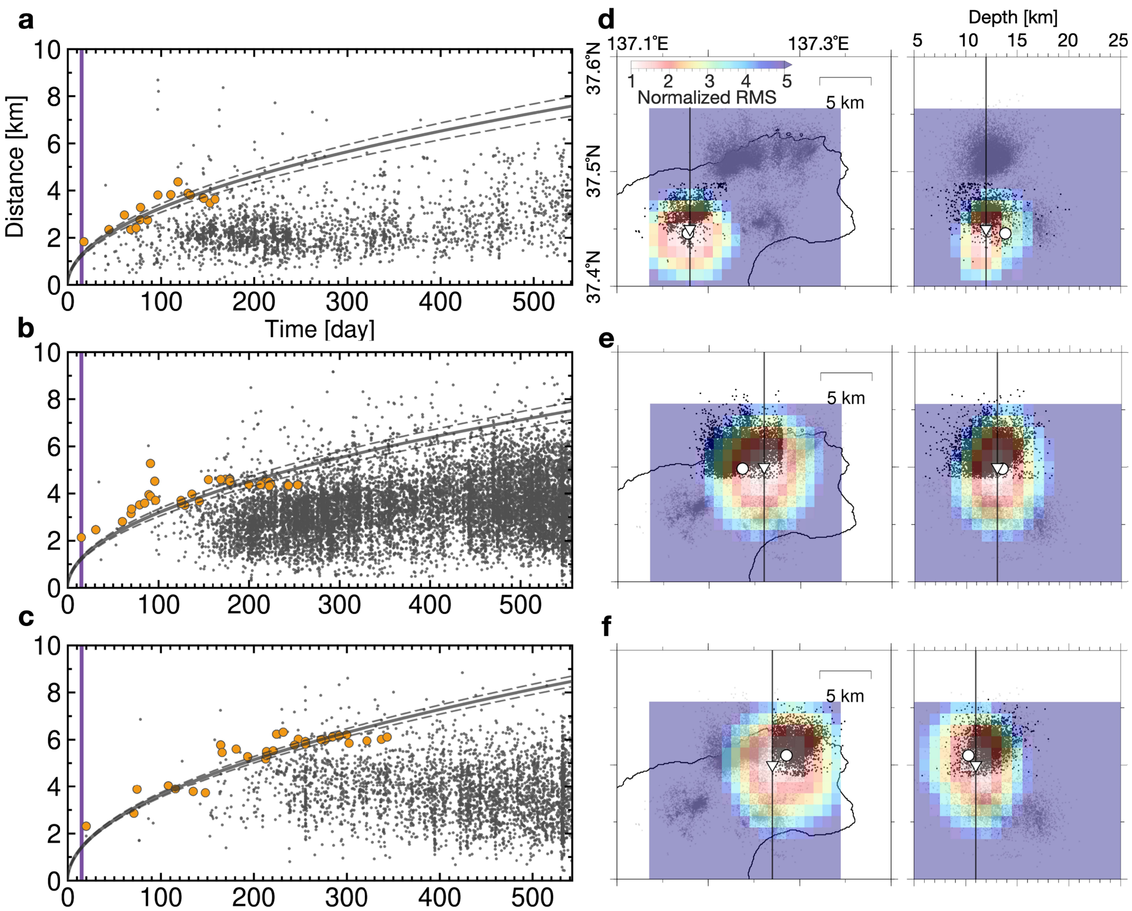

Figure 2. Diffusive hypocenter migration observed in the W, N, and NE clusters. **a–c** Elapsed time versus distance plots of the seismicity in the W, N, and NE clusters, respectively. Orange circles indicate the 95th percentile distance for the theoretical curve fitting. Black solid lines indicate the theoretical curve of best fit; dashed lines indicate the theoretical curve of the best fit with diffusivity ± 2$\boldsymbol{\sigma}$. Purple lines indicate the timing of the first earthquake in each cluster. **d–f** Spatial distribution of RMS misfit to the diffusion model with spatial origin assigned to the 3D grids. The color denotes the normalized RMS by the minimum RMS. Inverted triangle and circle indicate the location of the grid with minimum RMS and hypocenter of the first event, respectively. Horizontal bars indicate the position of cross-section and map view. Black dots show the relocated hypocenters.

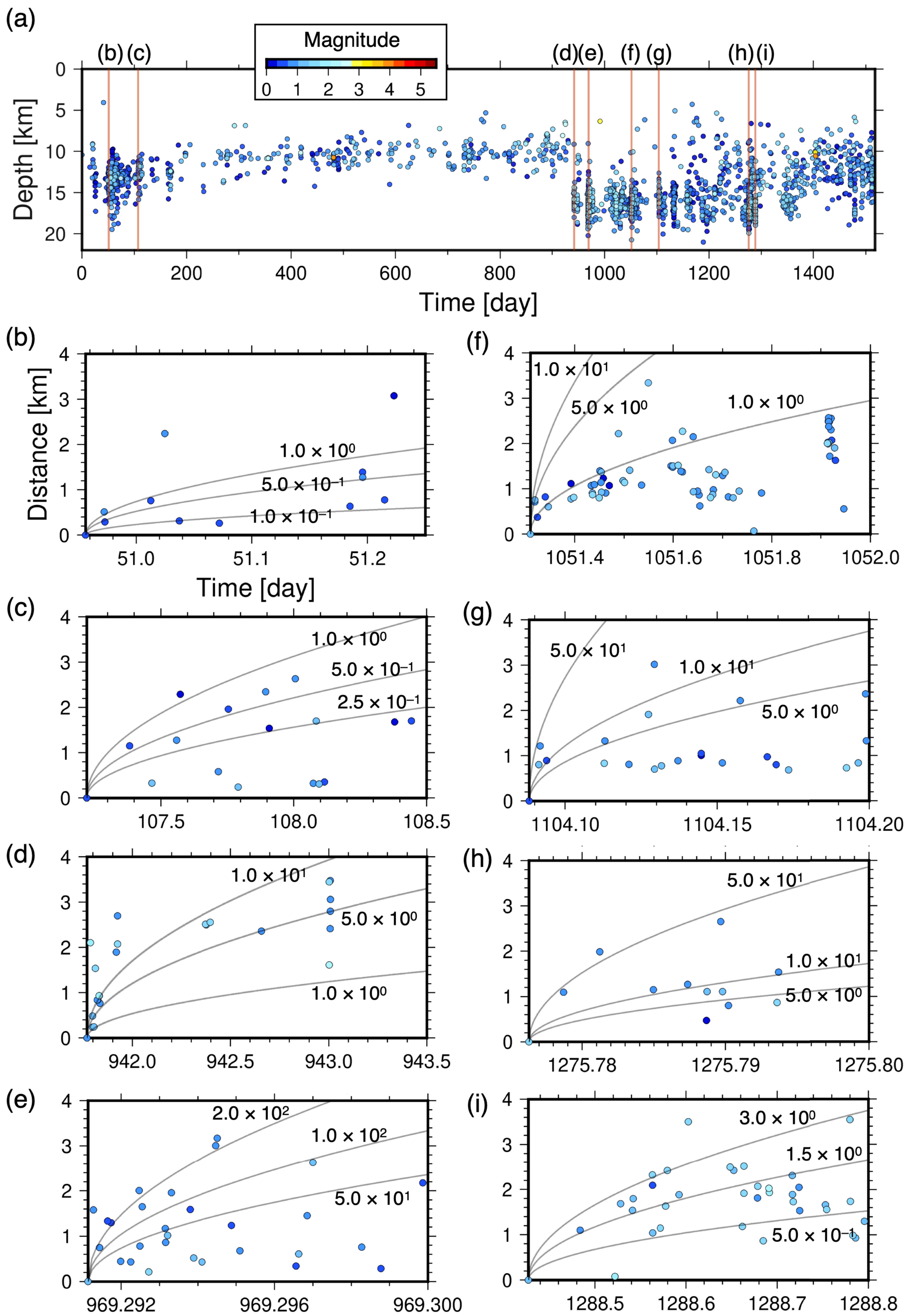

Figure 3. Intermittent seismicity in the S cluster and diffusive hypocenter migrations. **a** Temporal change in the seismicity of depth direction. The color represents the magnitude of each event. Red bars indicate intermittent seismic activities **b–i**. **b–i** Elapsed time versus distance plots of each intermittent activity. Gray solid lines show the theoretical curves for three different diffusivities: D [m^2/s] in each plot. The color of the circles indicates the magnitude.

4 Discussion and Conclusions

We observed diffusive hypocenter migrations in the swarm. Because diffusive hypocenter migration often occurs in swarms associated with anthropogenic fluid injection (Shapiro et al., 1997, 2002), our observations imply the presence of fluid in the swarm area. In addition, we found a corn-shaped hypocenter distribution in the deeper part of the S cluster (Figure 1(c), 1(d), and Movie S2 Supporting Information). This characteristic distribution is often present beneath volcanoes and is commonly interpreted as a circular dyke or the collapse of the chamber roof (Acocella, 2007). Although no volcanism has occurred around the swarm area since the Neogene (Ishiyama et al., 2017), there are hot springs with high geothermal gradients (Tanaka et al., 2004) and one with a high ^{3}He/^{4}He ratio (Umeda et al., 2009) near the swarm area. These facts support the inference that mantle-origin fluid exists beneath the swarm area. Recent findings in other studies on this swarm corroborate this suggestion; Nishimura et al. (2022) reported crustal deformation around the swarm— there has been 1.2 cm of horizontal displacement and 3.0 cm of uplift during the year since January 2021. They also reported an annual volumetric increase of approximately 2.5×10^7 m^3 at a depth of approximately 12 km, assuming a spherical inflation source. Nakajima (2022) performed seismic travel-time tomography around the swarm area and detected a low-velocity anomaly just beneath the S cluster. Considering these facts, we suggest that this swarm is plausibly driven by fluid stored beneath the S cluster migrating through the fractures created by Neogene volcanism.

The swarm was initiated in the S cluster and intensified after the end of December 2020 (Figure 1, Movie S1 in Supporting Information). We divided the swarm activity into two stages: precursor activity below 5 km depth of the S cluster (Figure 4(a), periods (1) and (2)), and subsequent intense activity involving novel seismicity in other clusters (Figure 4(a), period (3)). Herein, we discuss a plausible mechanism for this two-stage activation. As mentioned prior, we believe that a main driving factor of this swarm is the decrease in effective normal stress due to the intrusion of over-pressurized fluid from depth below the S cluster. Figure 4(b–d) shows the inferred principal stress profiles during the sequence and Mohr’s circle diagrams at two representative depths (see Text S1 in Supporting Information for detailed analysis). In the early stage of the precursor activity ((1) in Figure 4(a)), fluid supply from more than 15 km deep causes an increase in pore fluid pressure at a depth of approximately 15 km, initiating swarm activity. The stress conditions at this stage are shown in Figure 4(b). Subsequent fluid supply further increases the pore fluid pressure within the S cluster, which changes the stress condition, as shown in Figure 4(c), to that in Figure 4(d) (namely, the increase in the pore fluid pressure ratio, $\boldsymbol{\lambda}$). This model explains the migration of swarm activity to the shallower area (5–10 km) in the S cluster ((2) in Figure 4(a)). As time passes, the pore fluid pressure eventually exceeds the minimum principal stress (σ_3) at depth (Figure 4(d)), which widens the pre-existing fractures.

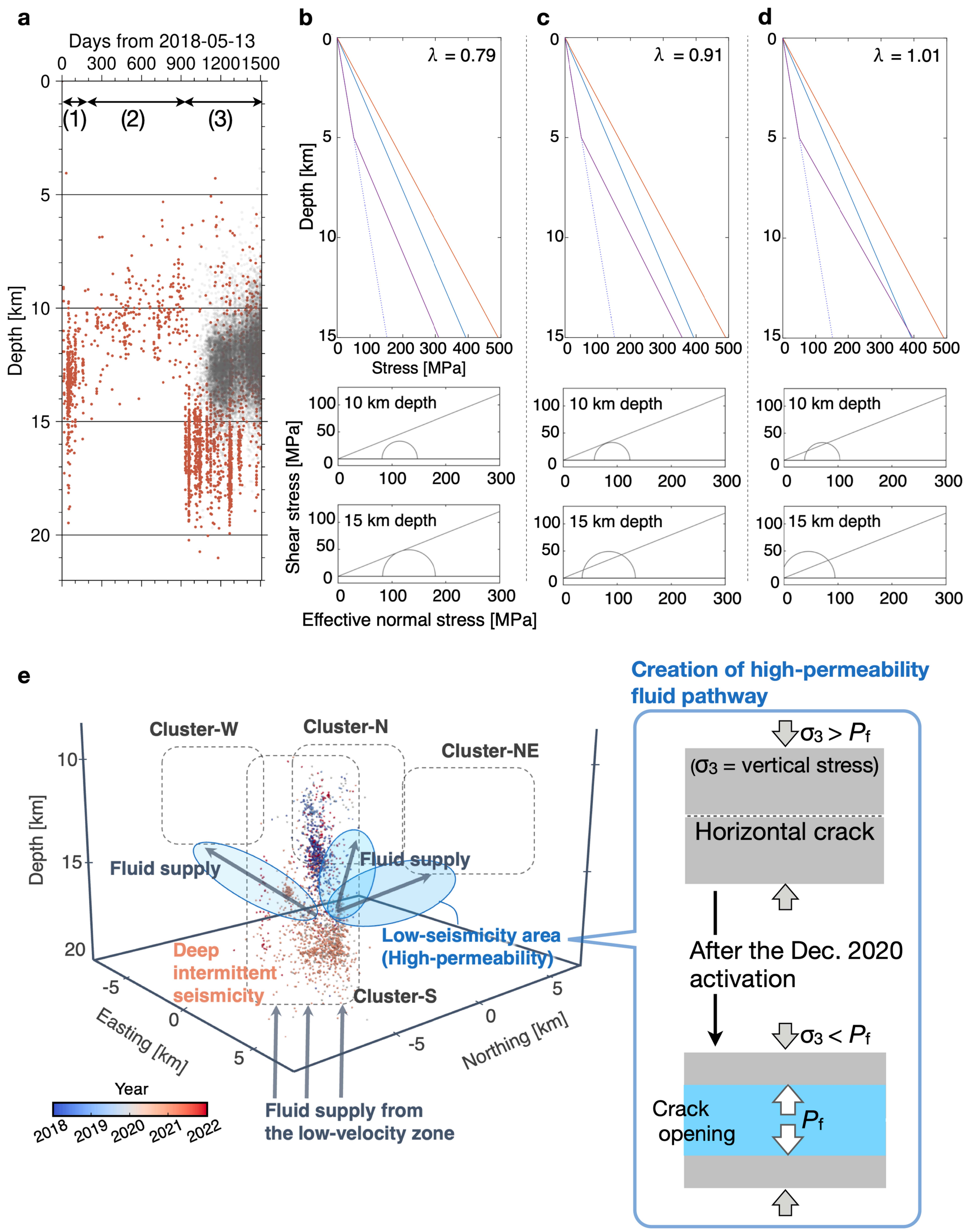

Figure 4. Comparing the temporal change in the seismicity with the stress state of depth direction. **a** The red dots and gray translucent dots indicate seismicity in the S cluster and other clusters, respectively. **b–d** Stress magnitude in the depth direction (upper panel) and Mohr's circle for 10 and 15 km depths (two lower panels). Red, blue, and purple solid lines and the dotted line indicate the changes in the maximum principal stress, minimum principal stress, pore

fluid pressure, and hydrostatic pressure in the depth direction, respectively. $\boldsymbol{\lambda}$ in upper panels indicates the pore fluid pressure ratio. **e** Diagram showing the spatial relationship between the S cluster (dots colored in time order) and other clusters (left image) and fluid pathway creation (right image).

The reverse fault-type focal mechanism solutions (Figure 1) suggest that the minimum principal stress axis is vertical. We infer that the open cracks both created the pathways of fluid supply and allowed additional supply between the S cluster and the surrounding areas, which enhanced the novel swarm activities in the other clusters ((3) in Figure 4(a)). Figure 4(e) shows a schematic diagram of the swarm activity with respect to the creation of fluid pathways and spatiotemporal swarm development. Sill-like horizontal cracks may have formed in the area due to the increased pore fluid pressure. In this stage, the fluid dissipated toward the other clusters, thus reducing the pore pressure and quiescing the seismic activity in the initial S cluster area (10–15 km depth) (Figure 4(a), 4(e)). Approximately 50 days after the initiation of intense activity in cluster S, novel seismic activities began in the W, N, and NE clusters beyond approximately 5 km of low-seismicity areas (Figure 1, Figure 4(a)). If fluid migrated through these low-seismicity areas, assuming density is 10^3 kg/m^3 and dynamic viscosity is 10^{-3} Pa·s (e.g., Talwani et al., 2007), the permeability would be on the order of 10^{-8} m^2. This value is notable higher than the seismogenic permeability (5×10^{-16} to 5×10^{-14} m^2) estimated for injection-induced seismicity (Talwani et al., 2007). This high permeability implies that rapid, aseismic fluid flow is occurring in these areas.

The swarm exhibits diffusive hypocenter migrations with varying diffusivities. According to previous studies that compiled the diffusivities with earthquake swarms (Talwani et al., 2007; Chen & Shearer, 2012; Amezawa et al., 2021), the diffusivities estimated for the W, N, and NE cluster are moderate to low. These values are smaller than the diffusivities estimated for swarms around active volcanoes (e.g., Yukutake et al., 2011; Shelly et al., 2016). This suggests that swarms in the W, N, and NE clusters have been driven by relatively slow pore fluid pressure diffusion in a low-permeability environment. Ross et al. (2020) imaged the fine 3-D spatiotemporal development of a long-living earthquake swarm in Cahuilla, California. They found strike-parallel channels of relatively high seismicity with hundreds of meters of vertical separation and suggested that a 3-D heterogeneous permeability structure with sub-horizontal permeability barriers in the fault zone controlled the slow spatiotemporal development of the swarm. We also found multiple clear planar hypocenter distributions, such as the one in the N cluster (Figure 1(d) and Movie S3 in Supporting Information). This situation is very similar to that in the Cahuilla swarm and implies strong spatial heterogeneity in the permeability structure in this area. This may be one of the factors contributing to the longevity of the swarm. On the contrary, many intermittent seismic activities in the S cluster showed rapid hypocenter migration with high diffusivity (10^1–10^2 m^2/s) (Figure 3(d), 3(e), 3(g), 3(h)). This is greater than the hypocenter migration associated with the common earthquake swarms described above (10^{-3}–10^1 m^2/s), and less than the diffusion speed of migration of slow earthquakes (10^3–10^5 m^2/s) observed at plate boundaries (e.g., Ide, 2010; Kato & Nakagawa, 2020). The former is thought to be related to spatiotemporal changes in pore fluid pressure, including fluid flow (e.g., Yukutake et al., 2011; Shelly et al., 2016), while the latter is thought to reflect stress diffusion (e.g., Ando et al., 2012). Thus, intermittent diffusive seismic activities in the S cluster may be a hybrid of both physical processes or simply the rapid fluid flow in a high-permeability environment. Quantitatively evaluating these processes and their interactions is open for the future work.

The intermittent seismic activity in the much deeper part of cluster S is critically important for understanding this long-living earthquake swarm. We observed rapid diffusive hypocenter migrations, especially after the activation of deep seismicity. Each burst of activity ceased within ten minutes (Figure 3). As mentioned above, these rapid diffusive migrations are related to not only diffusive spatiotemporal changes in the stress field, but also diffusive pore fluid pressure changes due to the release of highly pressurized fluid. Furthermore, the geothermal gradient of 80 K/km near the swarm area (Tanaka et al., 2004) and deep hypocenter distribution (Figure 1(d)) suggest that intermittent seismic activity occurs under a temperature and pressure environment on the order of 10^2 °C and 10^2 MPa, respectively. Thus, we propose two reasons for the intermittent seismic activity: the first is due to the high confining pressure around the deeper part of the S cluster (at least 350 MPa in 15–20 km); as soon as the fluid pressure diffuses, the effective normal stress reduction becomes inadequate for fault failure. The second is the rapid recovery of fault strength due to silica precipitation caused by abrupt depressurization when earthquakes occur (e.g., Weatherley & Henley, 2013; Ujiie et al., 2018; Amagai et al., 2019).

These intermittent seismic activities cause the geyser-like fluid supply from the S cluster to diffuse toward the other clusters through the high-permeability (low-seismicity) areas discussed above. In addition, the relatively small diffusivities observed in the W, N, and NE clusters suggests that once the supplied fluid reaches these areas, its dispersal is slowed by the relatively low permeability, allowing the pore fluid pressure to increase such that seismic activity escalates. Thus, the geyser-like fluid supply from beneath the S cluster coupled with the relatively low-permeability in the other cluster areas has made this swarm a long-living one.

Acknowledgments

We would like to thank Dr. Kodai Sagae of the Geological Survey of Japan, the National Institute of Advanced Industrial Science and Technology for his valuable discussions. This study was partly supported by JSPS KAKENHI Grant Number 22K19949.

Open Research

Data Availability Statement

We used hypocenter catalog data provided by the Japan Meteorological Agency (available at https://www.data.jma.go.jp/eqev/data/daily_map/index.html) and the F-net (National Research Institute for Earth Science and Disaster Resilience, 2019a) CMT catalog (https://www.fnet.bosai.go.jp). We also used seismographs observed by the Hi-net (National Research Institute for Earth Science and Disaster Resilience, 2019b), the Japan Meteorological Agency, Kyoto University, and the University of Tokyo. The seismographs were downloaded from the Hi-net website (https://hinetwww11.bosai.go.jp). The figures in this paper were generated using Generic Mapping Tools (Wessel et al., 2019; https://www.generic-mapping-tools.org). Topographic data used to construct figures were obtained from SRTM15+V2.1 (Tozer et al., 2019). The hypocenter catalog used in this study is available as Dataset S1 in the Supporting Information.

References

Acocella, V. (2007). Understanding caldera structure and development: An overview of analogue models compared to natural calderas. *Earth-Science Reviews*, *85*(3-4), 125–160. https://doi.org/10.1016/j.earscirev.2007.08.004

Amagai, T., Okamoto, A., Niibe, T., Hirano, N., Motomiya, K., & Tsuchiya, N. (2019). Silica nanoparticles produced by explosive flash vaporization during earthquakes. *Scientific reports*, *9*(1), 1–9. https://doi.org/10.1038/s41598-019-46320-7

Amezawa, Y., Maeda, T., & Kosuga, M. (2021). Migration diffusivity as a controlling factor in the duration of earthquake swarms. *Earth, Planets and Space*, *73*(1), 1–11. https://doi.org/10.1186/s40623-021-01480-7

Ando, R., Takeda, N., & Yamashita, T. (2012). Propagation dynamics of seismic and aseismic slip governed by fault heterogeneity and Newtonian rheology. *Journal of Geophysical Research: Solid Earth*, *117*(B11). https://doi.org/10.1029/2012JB009532

Byerlee, J. (1978). Friction of Rocks. *Pure and Applied Geophysics*. 116 (4-5): 615–626. https://doi.org/10.1007/BF00876528

Cappa, F., Rutqvist, J., & Yamamoto, K. (2009). Modeling crustal deformation and rupture processes related to upwelling of deep CO2-rich fluids during the 1965–1967 Matsushiro earthquake swarm in Japan. *Journal of Geophysical Research: Solid Earth*, *114*(B10). https://doi.org/10.1029/2009JB006398

Chen, X., & Shearer, P. M. (2011). Comprehensive analysis of earthquake source spectra and swarms in the Salton Trough, California. *Journal of Geophysical Research: Solid Earth*, *116*(B9). https://doi.org/10.1029/2011JB008263

Chen, X., Shearer, P. M., & Abercrombie, R. E. (2012). Spatial migration of earthquakes within seismic clusters in Southern California: Evidence for fluid diffusion. *Journal of Geophysical Research: Solid Earth*, *117*(B4). https://doi.org/10.1029/2011JB008973

Dublanchet, P., & De Barros, L. (2021). Dual seismic migration velocities in seismic swarms. *Geophysical Research Letters*, *48*(1). https://doi.org/10.1029/2020GL090025

Hagiwara, T., & Iwata, T. (1968). Summary of the seismographic observation of Matsushiro swarm earthquakes, *Bulletin of the Earthquake Research Institute, University of Tokyo*, *46*, 485–515. https://doi.org/10.15083/0000033433

Hauksson, E., Ross, Z. E., & Cochran, E. (2019). Slow-growing and extended-duration seismicity swarms: Reactivating joints or foliations in the Cahuilla Valley pluton, central Peninsular Ranges, Southern California. *Journal of Geophysical Research: Solid Earth*, *124*(4), 3933-3949. https://doi.org/10.1029/2019JB017494

Horton, S. (2012). Disposal of hydrofracking waste fluid by injection into subsurface aquifers triggers earthquake swarm in central Arkansas with potential for damaging earthquake. *Seismological Research Letters*, *83*(2), 250-260. https://doi.org/10.1785/gssrl.83.2.250

Ide, S. (2010). Striations, duration, migration and tidal response in deep tremor. *Nature*, *466*(7304), 356–359. https://doi.org/10.1038/nature09251

Ishiyama, T., Sato, H., Kato, N., Koshiya, S., Abe, S., Shiraishi, K., & Matsubara, M. (2017). Structures and active tectonics of compressionally reactivated back-arc failed rift across the Toyama trough in the Sea of Japan, revealed by multiscale seismic profiling. *Tectonophysics*, *710*, 21–36. https://doi.org/10.1016/j.tecto.2016.09.029

Jenatton, L., Guiguet, R., Thouvenot, F., & Daix, N. (2007). The 16,000-event 2003–2004 earthquake swarm in Ubaye (French Alps). *Journal of Geophysical Research: Solid Earth*, *112*(B11). https://doi.org/10.1029/2006JB004878

Kato, A., & Nakagawa, S. (2020). Detection of deep low-frequency earthquakes in the Nankai subduction zone over 11 years using a matched filter technique. *Earth, Planets and Space*, *72*(1), 1–9. https://doi.org/10.1186/s40623-020-01257-4

Lohman, R. B., & McGuire, J. J. (2007). Earthquake swarms driven by aseismic creep in the Salton Trough, California. *Journal of Geophysical Research: Solid Earth*, *112*(B4). https://doi.org/10.1029/2006JB004596

Mogi, K. (1963). Some discussions on aftershocks, foreshocks and earthquake swarms: the fracture of a semi-infinite body caused by an inner stress origin and its relation to the earthquake phenomena (third paper). *Bulletin of the Earthquake Research Institute, University of Tokyo*, *41*(3), 615–658. https://doi.org/10.15083/0000033716

Nakajima, J. (2022). Crustal structure beneath earthquake swarm in the Noto peninsula, Japan. *Earth, Planets and Space*, *74*(1), 1–11. https://doi.org/10.1186/s40623-022-01719-x

National Research Institute for Earth Science and Disaster Resilience (2019a). NIED F-net, National Research Institute for Earth Science and Disaster Resilience, https://doi.org/10.17598/nied.0005

National Research Institute for Earth Science and Disaster Resilience (2019b). NIED Hi-net, National Research Institute for Earth Science and Disaster Resilience, https://doi.org/10.17598/nied.0003

Nishimura, T., Nishikawa, T., Sato, D., Hiramatu, Y., & Sawada, A. (2022). Ongoing crustal deformation and earthquake swarm in the Noto Peninsula, central Japan, *EGU General Assembly 2022*, *Vienna*, *Austria*, *23–27 May 2022*, EGU22-10652. https://doi.org/10.5194/egusphere-egu22-10652

Ross, Z. E., Cochran, E. S., Trugman, D. T., & Smith, J. D. (2020). 3D fault architecture controls the dynamism of earthquake swarms. *Science*, *368*(6497), 1357–1361. https://doi.org/10.1126/science.abb0779

Ross, Z. E., & Cochran, E. S. (2021). Evidence for latent crustal fluid injection transients in Southern California from long-duration earthquake swarms. *Geophysical Research Letters*, *48*(12), e2021GL092465. https://doi.org/10.1029/2021GL092465

Shapiro, S. A., Huenges, E., & Borm, G. (1997). Estimating the crust permeability from fluid-injection-induced seismic emission at the KTB site. *Geophysical Journal International*, *131*(2), F15–F18. https://doi.org/10.1111/j.1365-246X.1997.tb01215.x

Shapiro, S. A., Rothert, E., Rath, V., & Rindschwentner, J. (2002). Characterization of fluid transport properties of reservoirs using induced microseismicity. *Geophysics*, *67*(1), 212–220. https://doi.org/10.1190/1.1451597

Shelly, D. R., Ellsworth, W. L., & Hill, D. P. (2016). Fluid-faulting evolution in high definition: Connecting fault structure and frequency-magnitude variations during the 2014 Long Valley Caldera, California, earthquake swarm. *Journal of Geophysical Research: Solid Earth*, *121*(3), 1776–1795. https://doi.org/10.1002/2015JB012719

Talwani, P., Chen, L., & Gahalaut, K. (2007). Seismogenic permeability, k_s. *Journal of Geophysical Research: Solid Earth*, *112*(B7). https://doi.org/10.1029/2006JB004665

Tanaka, A., Yamano, M., Yano, Y., & Sasada, M. (2004). Geothermal gradient and heat flow data in and around Japan (I): Appraisal of heat flow from geothermal gradient data. *Earth, Planets and Space*, *56*(12), 1191-1194. https://doi.org/10.1186/BF03353339

Terakawa, T., & Matsu'ura, M. (2010). The 3-D tectonic stress fields in and around Japan inverted from centroid moment tensor data of seismic events. *Tectonics*, *29*(6). https://doi.org/10.1029/2009TC002626

Thouvenot, F., Jenatton, L., Scafidi, D., Turino, C., Potin, B., & Ferretti, G. (2016). Encore ubaye: earthquake swarms, foreshocks, and aftershocks in the Southern French Alps. *Bulletin of the Seismological Society of America*, *106*(5), 2244–2257. https://doi.org/10.1785/0120150249

Toda, S., Stein, R. S., & Sagiya, T. (2002). Evidence from the AD 2000 Izu islands earthquake swarm that stressing rate governs seismicity. *Nature*, *419*(6902), 58–61. https://doi.org/10.1038/nature00997

Tozer, B., Sandwell, D. T., Smith, W. H. F., Olson, C., Beale, J. R., & Wessel, P. (2019). Global bathymetry and topography at 15 arc sec: SRTM15+. *Earth and Space Science*, *6*(10), 1847–1864. https://doi.org/10.1029/2019EA000658

Ueno, H., Hatakeyama, S., Aketagawa, T., Funasaki, J., & Hamada, N. (2002). Improvement of hypocenter determination procedures in the Japan Meteorological Agency, *Quarterly journal of seismology*, *65*, 123–134. (in Japanese with English abstract and figure caption)

Ujiie, K., Saishu, H., Fagereng, Å., Nishiyama, N., Otsubo, M., Masuyama, H., & Kagi, H. (2018). An explanation of episodic tremor and slow slip constrained by crack-seal veins and viscous shear in subduction mélange. *Geophysical Research Letters*, *45*(11), 5371–5379. https://doi.org/10.1029/2018GL078374

Umeda, K., Ninomiya, A., & Negi, T. (2009). Heat source for an amagmatic hydrothermal system, Noto Peninsula, Central Japan. *Journal of Geophysical Research: Solid Earth*, *114*(B1). https://doi.org/10.1029/2008JB005812

Vidale, J. E., Boyle, K. L., & Shearer, P. M. (2006). Crustal earthquake bursts in California and Japan: Their patterns and relation to volcanoes. *Geophysical Research Letters*, *33*(20). https://doi.org/10.1029/2006GL027723

Waldhauser, F., & Ellsworth, W. L. (2000). A double-difference earthquake location algorithm: Method and application to the northern Hayward fault, California. *Bulletin of the seismological society of America*, *90*(6), 1353-1368. https://doi.org/10.1785/0120000006

Weatherley, D. K., & Henley, R. W. (2013). Flash vaporization during earthquakes evidenced by gold deposits. *Nature Geoscience*, *6*(4), 294–298. https://doi.org/10.1038/ngeo1759

Wessel, P., Luis, J. F., Uieda, L., Scharroo, R., Wobbe, F., Smith, W. H. F., & Tian, D. (2019). The Generic Mapping Tools version 6. *Geochemistry, Geophysics, Geosystems*, *20*, 5556–5564. https://doi.org/10.1029/2019GC008515

Yoshida, K., Saito, T., Urata, Y., Asano, Y., & Hasegawa, A. (2017). Temporal changes in stress drop, frictional strength, and earthquake size distribution in the 2011 Yamagata-Fukushima, NE Japan, earthquake swarm, caused by fluid migration. *Journal of Geophysical Research: Solid Earth*, *122*(12), 10–379. https://doi.org/10.1002/2017JB014334

Yukutake, Y., Ito, H., Honda, R., Harada, M., Tanada, T., & Yoshida, A. (2011), Fluid-induced swarm earthquake sequence revealed by precisely determined hypocenters and focal mechanisms in the 2009 activity at Hakone volcano, Japan. *Journal of Geophysical Research: Solid Earth*, *116*(B4). https://doi.org/10.1029/2010JB008036

Zoback, M. D., & Townend, J. (2001). Implications of hydrostatic pore pressures and high crustal strength for the deformation of intraplate lithosphere. *Tectonophysics*, *336*(1-4), 19–30. https://doi.org/10.1016/S0040-1951(01)00091-9

Figure 1.

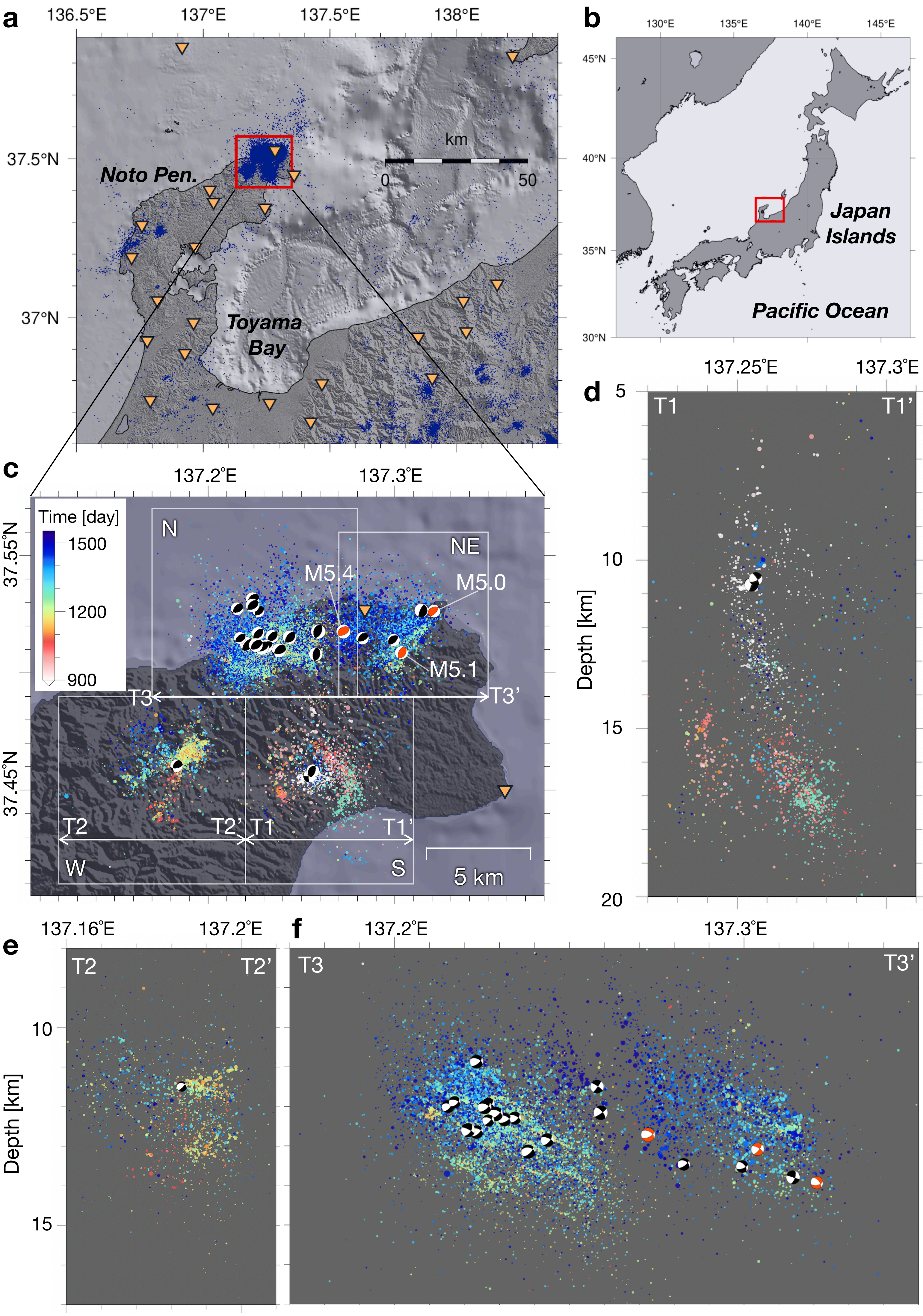

a
136.5°E
137°E
137.5°E
138°E
37.5°N
37°N
Noto Pen.
Toyama Bay
km
0
50
b
130°E
135°E
140°E
145°E
45°N
40°N
35°N
30°N
Japan Islands
Pacific Ocean
c
137.2˚E
137.3˚E
37.55˚N
37.45˚N
Time [day]
1500
1200
900
N
NE
M5.4
M5.0
M5.1
T3
T3'
T2
T2'
T1
T1'
W
S
5 km
d
137.25˚E
137.3˚E
T1
T1'
Depth [km]
5
10
15
20
e
137.16˚E
137.2˚E
T2
T2'
Depth [km]
10
15
f
137.2˚E
137.3˚E
T3
T3'

Figure 2.

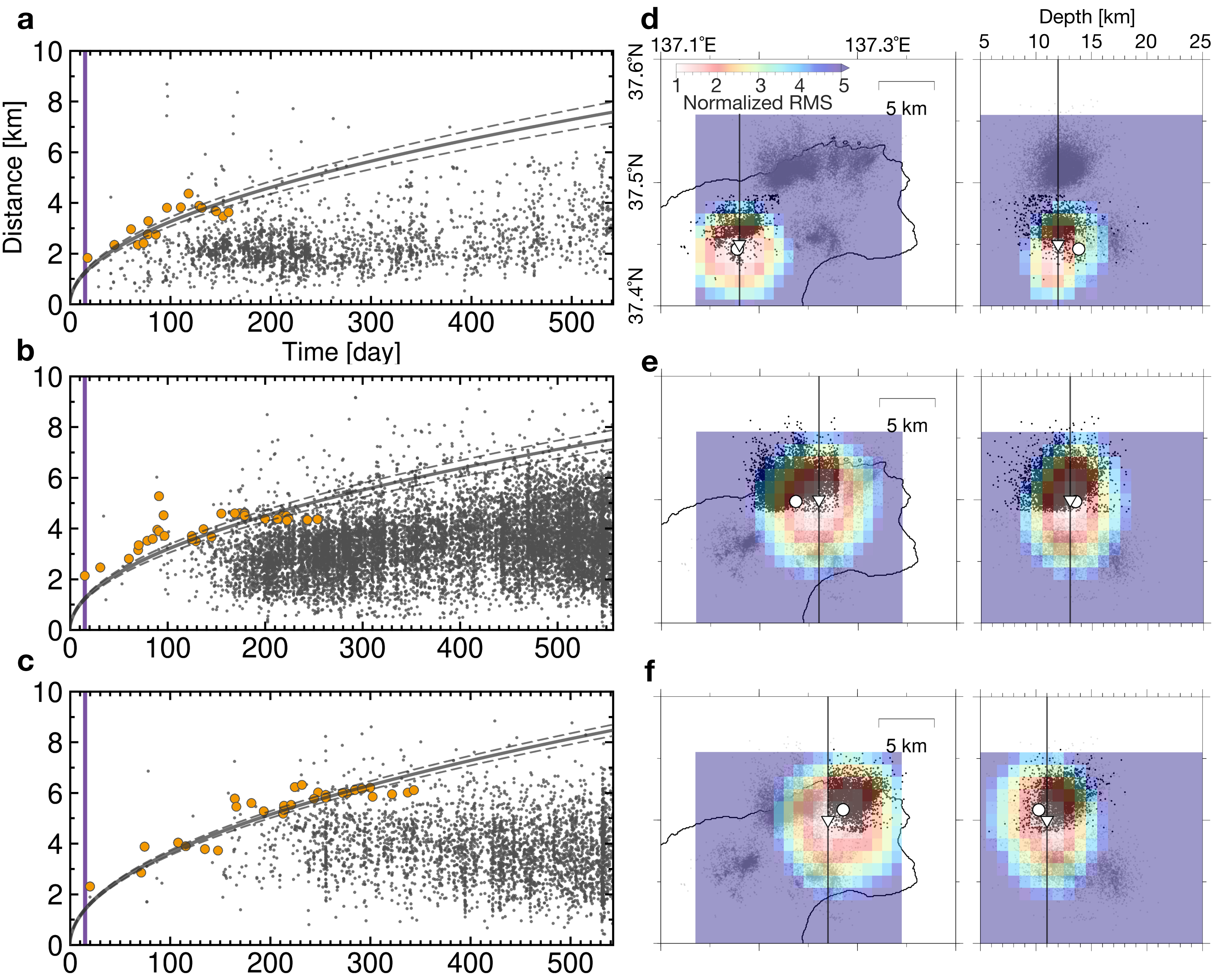

a
b
c
d
e
f
Distance [km]
Time [day]
Depth [km]
137.1°E
137.3°E
37.6°N
37.5°N
37.4°N
Normalized RMS
5 km

Figure 3.

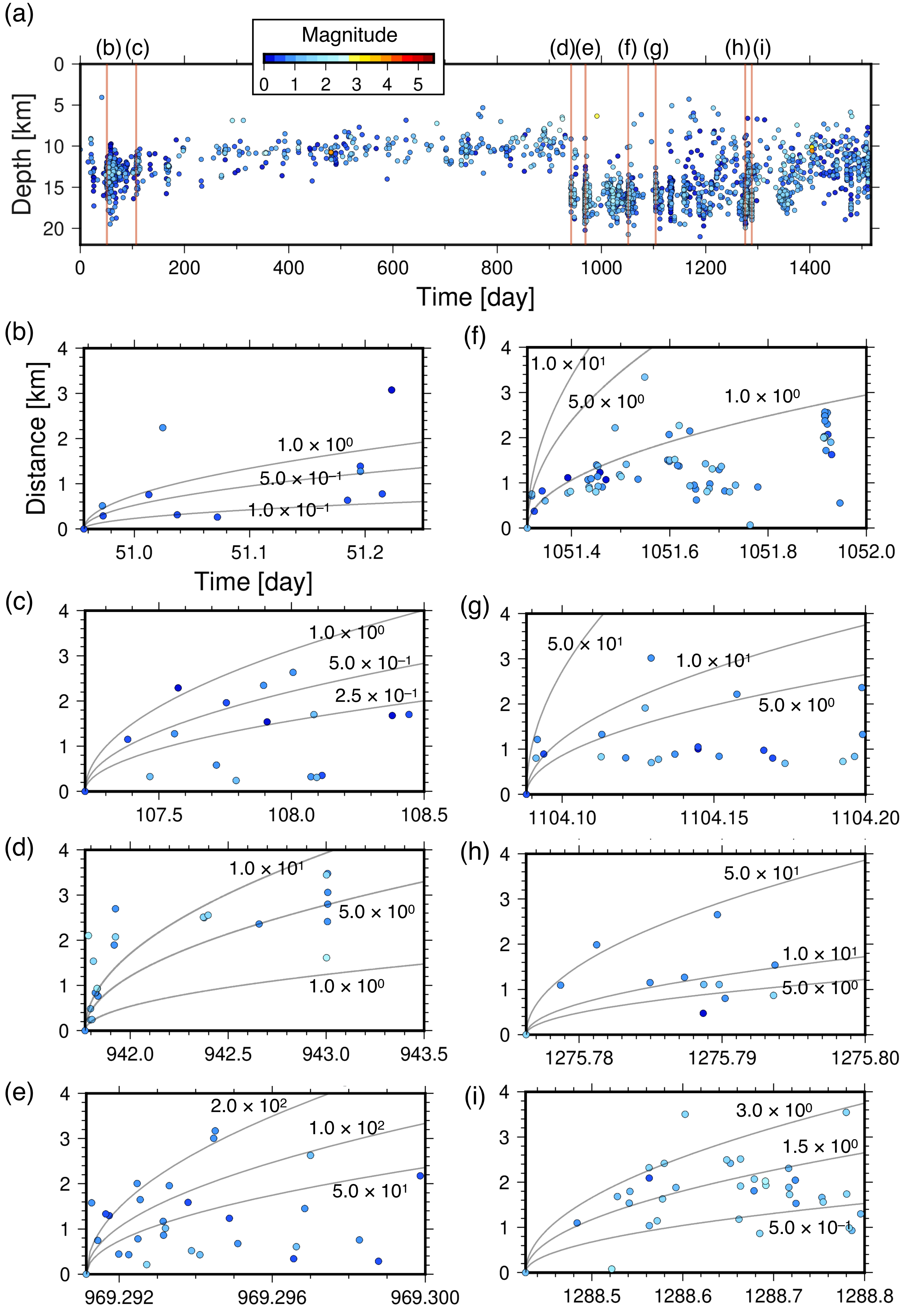
(a)
Magnitude
0 1 2 3 4 5
(b) (c) (d)(e) (f) (g) (h)(i)
Depth [km]
Time [day]
(b)
Distance [km]
Time [day]
1.0 × 10^0
5.0 × 10^−1
1.0 × 10^−1
(c)
1.0 × 10^0
5.0 × 10^−1
2.5 × 10^−1
(d)
1.0 × 10^1
5.0 × 10^0
1.0 × 10^0
(e)
2.0 × 10^2
1.0 × 10^2
5.0 × 10^1
(f)
1.0 × 10^1
5.0 × 10^0
1.0 × 10^0
(g)
5.0 × 10^1
1.0 × 10^1
5.0 × 10^0
(h)
5.0 × 10^1
1.0 × 10^1
5.0 × 10^0
(i)
3.0 × 10^0
1.5 × 10^0
5.0 × 10^−1

Figure 4.

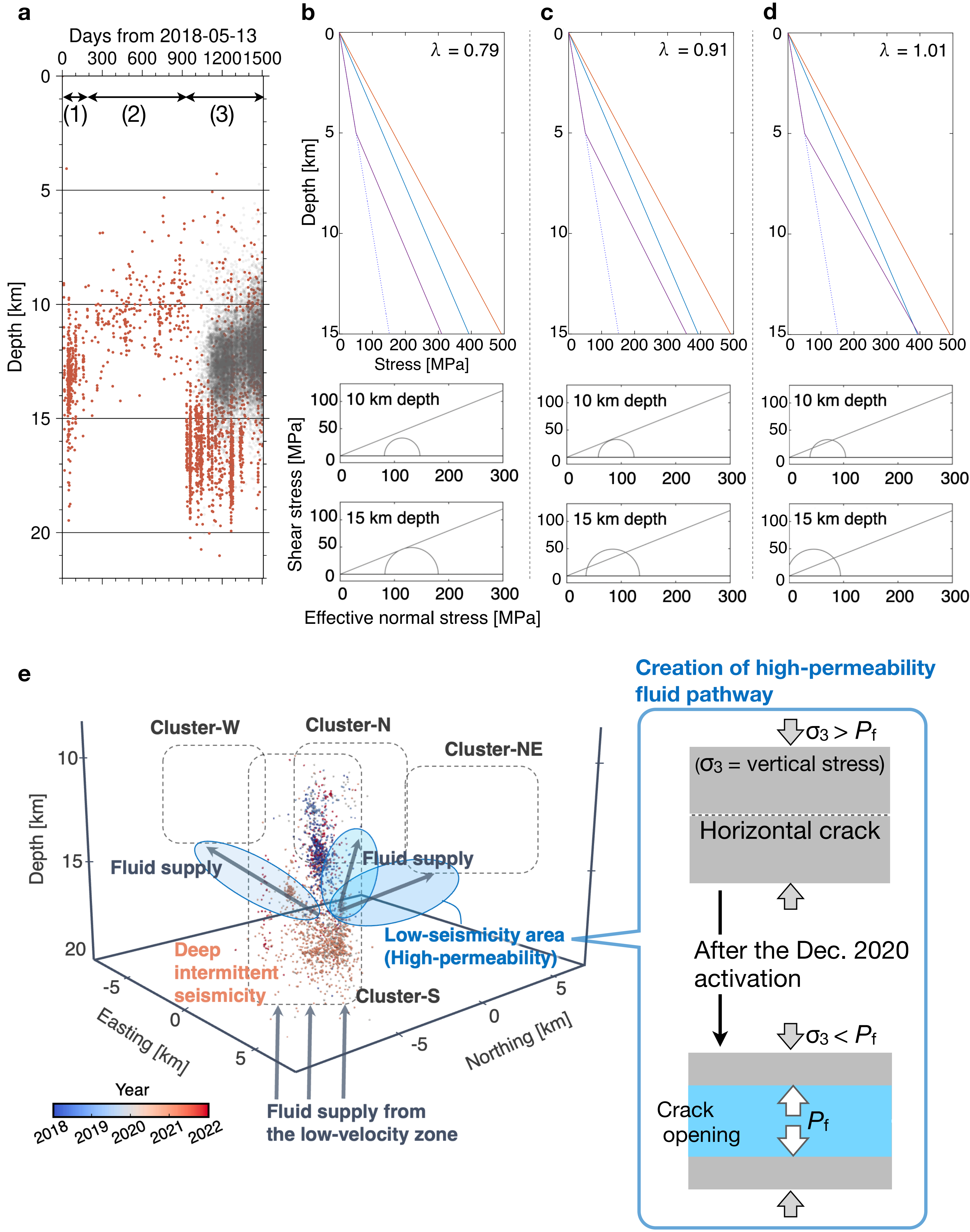

a
Days from 2018-05-13
0 300 600 900 1200 1500
(1) (2) (3)
Depth [km]
b
λ = 0.79
Depth [km]
Stress [MPa]
c
λ = 0.91
d
λ = 1.01
10 km depth
15 km depth
Shear stress [MPa]
Effective normal stress [MPa]
e
Cluster-W
Cluster-N
Cluster-NE
Cluster-S
Fluid supply
Fluid supply
Low-seismicity area
(High-permeability)
Deep
intermittent
seismicity
Depth [km]
Easting [km]
Northing [km]
Year
2018 2019 2020 2021 2022
Fluid supply from
the low-velocity zone
Creation of high-permeability
fluid pathway
σ3 > Pf
(σ3 = vertical stress)
Horizontal crack
After the Dec. 2020
activation
σ3 < Pf
Crack
opening
Pf